Open access • Journal Article • DOI:10.1126/SCIENCE.1098454

Nanoparticles: Strained and Stiff — Source link

Benjamin Gilbert, Feng Huang, Hengzhong Zhang, Glenn A. Waychunas ...+2 more authors

Institutions: University of California, Berkeley, Lawrence Berkeley National Laboratory

Published on: 30 Jul 2004 - Science (American Association for the Advancement of Science)

Topics: Zinc sulfide

Nanoparticles: Strained and Stiff

Benjamin Gilbert[1], Feng Huang[1], Hengzhong Zhang[1], Glenn A. Waychunas[2], Jillian F. Banfield[1,2]*

[1]Department of Earth and Planetary Sciences, University of California at Berkeley, Berkeley, CA 94720, USA. [2]Earth Sciences Division, Lawrence Berkeley National Lab, One Cyclotron Road, Berkeley, CA 94720, USA.

*To whom correspondence should be addressed. Email: jill@eps.berkeley.edu

Abstract

Nanoparticles may contain unusual forms of structural disorder that can substantially modify materials properties and thus cannot solely be considered as small pieces of bulk material. We have developed a method to quantify intermediate-range order in 3.4-nanometer-diameter zinc sulfide nanoparticles and show that structural coherence is lost over distances beyond 2 nanometers. The zinc-sulfur Einstein vibration frequency in the nanoparticles is substantially higher than that in the bulk zinc sulfide, implying structural stiffening. This cannot be explained by the observed 1% radial compression and must be primarily due to inhomogeneous internal strain caused by competing relaxations from an irregular surface. The methods developed here are generally applicable to the characterization of nanoscale solids, many of which may exhibit complex disorder and strain.

The electronic properties of nanoparticles can differ from those of their corresponding bulk form due to confinement effects caused only by their finite size, and because they are structurally distinct. Quantum confinement is the dominant size effect, and has been well studied (*1*–*6*). Structural deviations in nanoparticles relative to bulk material are not well understood because they are hard to resolve experimentally (*7*). Consequently, theoretical models of nanoparticles generally assume they have bulklike interior structure (*8*). Tight-binding calculations that optimized nanoparticle structure, and assumed full theoretical passivation of surface anions, suggested that surfaces of nanoparticles relax in a manner comparable to that of bulk surfaces (*9*). However, classical and quantum molecular dynamics simulations have indicated that disorder may pervade throughout nanoparticles (*10*, *11*). We previously showed that nanoparticles can undergo substantial transformation in structure at low temperature, driven by surface interactions, indicating that internal strain depends upon the nature of the surroundings as well as size (*12*). However, a detailed description of the strain within nanoparticles has not been experimentally obtained. We combine pair distribution function and extended x-ray absorption fine structure (EXAFS) analyses to quantify the structural distortion within mercaptoethanol-coated zinc sulfide (ZnS) nanoparticles and the consequent changes in lattice dynamics.

Mercaptoethanol-coated ZnS nanoparticles were synthesized using the method of Vogel *et al.* (*13*). Fits to small-angle x-ray scattering (SAXS) data indicate that the average diameter is 3.4 nm with a full width at half maximum (FWHM) of 0.6 nm for the size distribution (Fig. 1), in close agreement with the size estimated from ultraviolet-visible absorption spectroscopy (fig. S1) (*14*). High-resolution transmission electron microscope (HRTEM) data confirm the size determined by SAXS and show that the nanoparticles are approximately spherical (fig. S2).

We acquired wide-angle x-ray scattering (WAXS) patterns from powders of bulk ZnS (sphalerite structure) and mercaptoethanol-coated ZnS nanoparticles (fig. S3). Although the WAXS patterns from the nanoparticles and from the bulk material have peaks in essentially the same positions (indicating that they share the same basic structure), the peaks from the nanoparticles are wider and less intense. We obtained the real-space interatomic distance correlation functions, commonly known as pair distribution functions (PDFs), from the WAXS data using standard methods (*14–17*). The PDFs of bulk ZnS and ZnS nanoparticles are given in Fig. 2A. The PDF reveals interatomic correlations at much greater distances than can be achieved by EXAFS (see below) (*18–20*). In contrast to Bragg peak analysis of diffraction data (*21*), the PDF additionally uses information from total diffuse x-ray scattering.

The nanoparticle PDF approaches zero at 2.0 nm rather than at 3.4 nm, indicating the presence of structural disorder. A detailed analysis of the disorder in the nanoparticles can be made by comparing the observed PDF to one obtained by truncating the PDF from bulk ZnS with a real-space curve associated with a 3.4-nm-diameter sphere (*14*, *22*). This operation creates the PDF of "ideal" ZnS sphalerite nanoparticles, also shown in Fig. 2A, allowing finite particle-size effects on the diffraction data to be separated from structural effects.

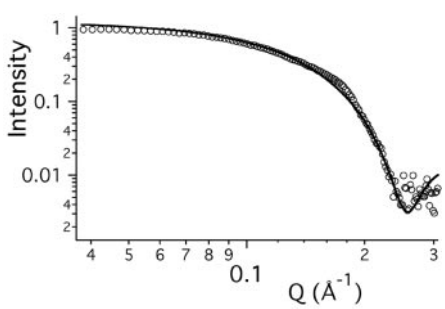

Fig. 1. Small-angle x-ray scattering (SAXS) data (circles) from mercaptoethanol-coated ZnS nanoparticles in aqueous solution. The fit (solid line) is for polydisperse dilute spheres of average diameter 3.4 nm and Schultz size distribution FWHM of 0.6 nm.

The PDF for real ZnS nanoparticles is distinct from that of ideal nanoparticles in the following respects: (i) The first-shell PDF peak intensity, representing Zn-S bonds throughout the nanoparticles, is lower for real than for ideal nanoparticles. (ii) PDF peak intensities at higher correlation distances diminish more rapidly in the real nanoparticles. (iii) PDF peak widths are broader in the real nanoparticles. (iv) PDF peak positions are shifted. Observations (i) to (iii) indicate the presence of two distinct forms of excess static disorder within the real nanoparticles relative to bulk sphalerite (Fig. 3, A and B). The low dependence on temperature of WAXS measurements (fig. S7) indicates that this excess disorder is structural (i.e., static disorder) rather than vibrational (i.e., thermal disorder). The reduction and broadening of all peaks in the PDF indicate that the random mean squared displacements about equilibrium positions (uncorrelated with the positions of neighboring atoms) are increased (Fig. 3A). However, this type of disorder broadens all peaks in the PDF equivalently and cannot explain the loss of intensity with increasing interatomic distance. Thus, a second effect is that strain within the nanoparticle causes correlated shifts in the equilibrium positions themselves, relative to the perfect sphalerite lattice (Fig. 3B). This effect is cumulative with increasing interatomic distance and causes peak intensities in the real nanoparticle PDF to vanish at a correlation length of about 2.0 nm.

In addition, observation (iv) indicates a contraction of nanoparticle bond lengths (Fig. 3C). We quantified the lattice contraction and the two types of disorder by fitting real-space interatomic correlations from the sphalerite structure to the experimental PDFs (*14*). From a fit to the bulk sphalerite data (fig. S5), we obtained the thermal contribution to PDF peak broadening by fitting the mean squared relative displacement (MSRD) while accounting empirically for correlated atomic motion (*23*). From a fit to the nanoparticle data that accounted for the nanoparticle size and incorporated the thermal MSRD value obtained from the bulk, we obtained two

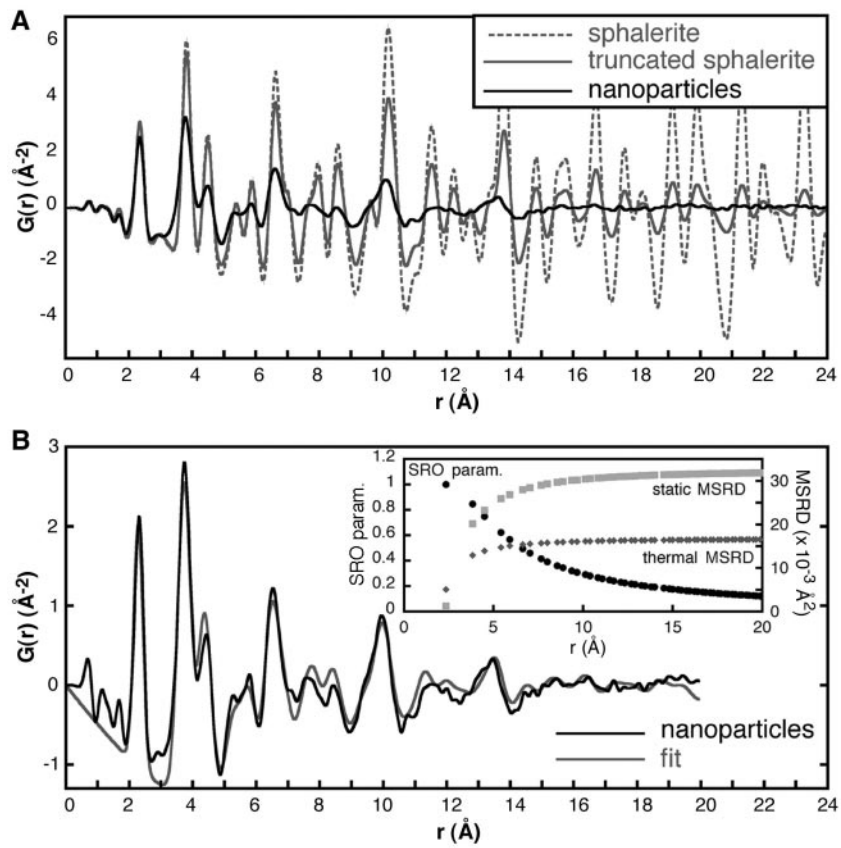

Fig. 2. (**A**) PDFs of bulk ZnS (sphalerite, dashed gray curve), bulk ZnS following truncation by the shape factor for a 3.4-nm-diameter sphere (gray curve), and mercaptoethanol-coated ZnS nanoparticles of average diameter 3.4 nm (black curve). (**B**) Theoretical fit (gray curve) to the PDF of ZnS nanoparticles (black curve), accounting for finite particle size and including the thermal mean square relative displacement (MSRD) obtained from a fit to the bulk sphalerite data (inset, diamonds). In addition, the fit includes a static harmonic disorder contribution to the MSRD (inset, squares) and a short-range order (SRO) parameter (inset, circles). The MSRD contributions broaden the PDF peaks; the SRO parameter is an intensity scaling factor.

additional static disorder parameters that have a dependence on interatomic distance, r. The first parameter is the static MSRD contribution to PDF peak broadening due to random displacements about equilibrium positions. The second is a short-range order parameter, $P^{SRO}(r)$, where $0 < P^{SRO} \leq 1$, that causes the loss of PDF peak intensity due to the correlated shifts in equilibrium positions. The best-fit results are given in Fig. 2B.

The static MSRD contribution is shown in the inset to Fig. 2B. Its form resembles that of the thermal MSRD (obtained from bulk ZnS) in that there is less disorder at short correlation lengths. For thermal disorder, this lineshape is due to correlated atomic motion (*23*). By analogy, the static disorder is also correlated over short distances.

The best-fit curve $P^{SRO}(r)$ approaches zero with increasing correlation distance. This shows that, at larger interatomic distances, fewer atoms maintain definite structural relationships relative to other atoms in the nanoparticle. This finding is consistent with preservation of short-range order, strong reduction in intermediate-range order, and complete loss of structural coherence at distances greater than 2 nm (*16*).

From the PDF fit, we measured a mean 1% radial contraction of interatomic correlations in the real nanoparticles. However, the peak shifts are more complex, as indicated by a plot of nanoparticle peak shift versus sphalerite peak position (Fig. 3C). From studies on a model nanoparticle subjected to structural modifications, we can show that simple models for internal strain can be distinguished by the shifts in the associated PDF peak positions (fig. S8). However, we conclude that the strain within the real nanoparticles is more complex than that described by any of the simple models that we considered, including uniform, or surface-weighted, radial strain; linear strain; or the presence of stacking faults.

The loss of structural coherence and the inability of simple strain models to describe peak shifts in PDF data point to the existence of complex strain fields within the nanoparticles. We infer that the pervasive internal distortion is due to strain that arises from the competing attempts of the structurally diverse terminating surfaces that encompass the nanoparticles to adopt lower energy configurations. Even with strong chemical passivation, nanoparticle surfaces are generally nonstoichiometric [because capping ligands interact with surface cations or anions only, e.g. (*20*)] and incompletely capped [due to steric limits, e.g. (*24*)]. The inherent limit of surface passivation creates structural effects throughout the nanoparticle interior, despite the highly crystalline appearance within the transmission electron micrographs (fig. S2) or from x-ray diffraction (fig. S3). We anticipate that the observed forms of disorder are general features of nanoscale solids and will be especially pronounced where there is minimal passivation.

Because internal strain and disorder can substantially affect materials properties, we investigated the lattice dynamics of the ZnS samples. We obtained Zn K-edge EXAFS spectra between 3 and 500 K from the same bulk ZnS and ZnS nanoparticles used in the PDF analysis (Fig. 4A and fig. S9). The EXAFS spectra from bulk ZnS contain peaks from long-range structure that are weak or absent in the spectra from the nanoparticles, even at low temperature.

We obtained the first-shell (Zn-S) MSRD as a function of temperature by fitting the data in Fig. 4A to ZnS scattering paths obtained through simulation using the FEFF code (*14*, *25*). In Fig. 4B, the nanoparticle MSRD curve is offset from that of the bulk, indicating the presence of excess static disorder in the nanoparticles. The room-temperature EXAFS and PDF analyses yield consistent measurements of this excess structural disorder. First-shell combined thermal and static MSRDs in bulk and nanoparticles are 5.1×10^{-3} Å^2 and 6.4×10^{-3} Å^2, respectively, from fits to the EXAFS data, and 5.0×10^{-3} Å^2 and 6.6×10^{-3} Å^2 from fits to the PDF data.

From Fig. 4B, the amplitudes of vibrations in bulk ZnS begin to increase rapidly with temperature at ~70 K, but this increase is not seen in the nanoparticles until ~130 K. This indicates structural stiffening in the nanoparticles.

We fitted the temperature response of the MSRD to a theoretical expression for the anharmonic Einstein oscillator (*14*, *26*). In the Einstein model, the Zn-S bonding pair is considered to vibrate in the center of mass

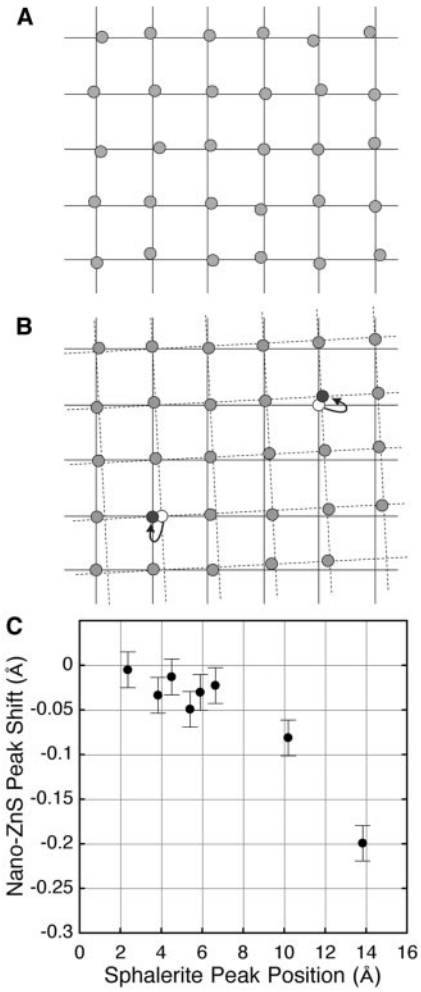

Fig. 3. Structural modifications in ZnS nanoparticles can be decomposed into two distinct disorder types, plus lattice contraction. (**A**) Random displacement disorder. Individual atoms are randomly displaced from sites on a single lattice. (**B**) Strain-driven distortion. Local structure is maintained, but at larger interatomic distances, atoms lie farther from the positions expected for an undistorted lattice. (**C**) Lattice contraction. The shift in PDF peak positions observed in ZnS nanoparticles is plotted against the positions of the equivalent peaks in the bulk sphalerite PDF.

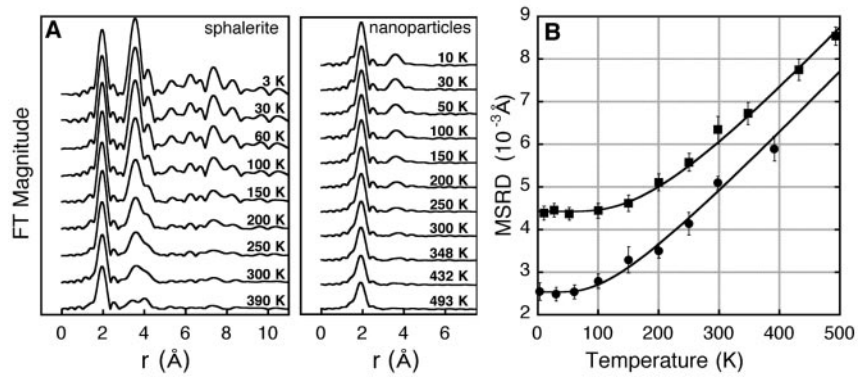

Fig. 4. (**A**) Fourier transform magnitude of k^3-weighted Zn K-edge EXAFS spectra of bulk ZnS (sphalerite) and ZnS nanoparticles as a function of temperature. (**B**) Temperature dependence of the first-shell mean square relative displacement (MSRD) obtained from fits to the EXAFS data. The lines are fits to the first-shell MSRD data using an anharmonic Einstein oscillator model to extract characteristic vibration frequencies for the two samples. A discussion of the errors in the MSRD determination is given in the Supporting Online Material (*14*).

frame under the influence of the interatomic potential of the remaining stationary lattice. The characteristic vibration frequency obtained for bulk ZnS is 7.12 ± 1.2 THz. This value is consistent with that reported previously for bulk CdSe (*27*, *28*). In comparison, the characteristic vibration frequency for the ZnS nanoparticles is 11.6 ± 0.4 THz. Although these values cannot be simply related to the full phonon dispersion relations for ZnS, the trend clearly indicates lattice stiffening. This implies that the heat capacity of the ZnS lattice, excluding surface-bound species, is lower in nanoparticles than in equivalent bulk material.

There are several features of the nanoparticles that may be responsible for the lattice stiffening. First, the PDF analysis indicates ~1% bond length compression. Because crystalline materials show an increase in vibration frequencies with pressure (away from phase transitions), the compression will cause lattice stiffening. However, compression of this magnitude alone cannot explain the large increase in vibration frequency. The average change in bond length provides an incomplete picture because disorder within the nanoparticles leads to a large distribution of bond lengths, and all deviations from the equilibrium bond lengths may increase the vibration frequency. We thus find that structural disorder is principally responsible for the lattice stiffening.

In summary, we quantitatively determined nanoparticle crystallinity and disorder, using a PDF-based method. We found that the best description of nanoparticle structure includes bond length contraction, random disorder, and a type of disorder characterized by correlated atomic displacements. The internal disorder is observed despite the presence of strongly bound surface ligands. We conclude that even with strong chemical passivation, surface atoms exist in diverse unsatisfied bonding environments at the surface that drive inhomogeneous internal strain. A striking consequence of the internal disorder is that the nanoparticles are much stiffer than expected from the measured bond length contraction. Our approach is an important step toward a realistic description of nanoparticle structure that includes internal strain, which is likely to be a general feature of nanoscale solids. Because lattice contraction and disorder will separately modify electronic properties, inclusion of these effects is essential for accurate nanoparticle calculations.

References and Notes

1. R. Rossetti, R. Hull, J. M. Gibson, L. E. Brus, *J. Chem. Phys.* **82**, 552 (1985).
2. C. B. Murray, D. J. Norris, M. G. Bawendi, *J. Am. Chem Soc.* **115**, 8706 (1993).
3. A. P. Alivisatos, *Science* **271**, 933 (1996).
4. L. E. Brus, *J. Chem. Phys.* **80**, 4403 (1984).
5. P. E. Lippens, M. Lannoo. *Phys. Rev. B* **39**, 10935 (1989).
6. A. Franceschetti, A. Zunger, *Phys. Rev. Lett.* **78**, 915 (1997).
7. B. Palosz *et al.*, *Z. Kristallogr.* **217**, 497 (2002).
8. L.-W. Wang, A. Zunger, *Phys. Rev. B* **53**, 9579 (1996).
9. K. Leung, K. B. Whaley, *J. Chem. Phys.* **110**, 11012 (1999).
10. E. Rabani, *J. Chem. Phys.* **115**, 1493 (2001).
11. A. Puzder, A. J. Williamson, F. A. Reboredo, G. Galli, *Phys. Rev. Lett.* **91**, 157405 (2003).
12. H. Zhang, B. Gilbert, F. Huang, J. F. Banfield. *Nature* **424**, 1025 (2003).
13. W. Vogel, P. H. Borse, N. Deshmukh, S. K. Kulkarni, *Langmuir* **16**, 2032 (2000).
14. See supporting online material.
15. B. J. Thijsse, *J. Appl. Crystallogr.* **17**, 61 (1984).
16. A. C. Wright *et al.*, *J. Non-Cryst. Solids* **129**, 213 (1991).
17. S. J. L Billinge, M. F. Thorpe, Eds., *Local Structure from Diffraction* (Plenum, New York, 1998).
18. J. Rockenburger, *et al. J. Chem. Phys.* **108**, 7807 (1998).
19. M. A. Marcus, W. Flood, M. Steigerwald, L. Brus, M. Bawendi. *J. Phys. Chem.* **95**, 1572 (1991).
20. A. C. Carter, *et al.*, *Phys. Rev. B* **55**, 13822 (1997).
21. M. G. Bawendi, A. R. Kortan, M. L. Seigerwald, L. E. Brus, *J. Chem. Phys.* **91**, 7282 (1989).
22. G. Mason, *Nature* **217**, 733 (1968).
23. I.-K. Jeong, Th. Proffen, F. Mohiuddin-Jacobs, S. J. L. Billinge, *J. Phys. Chem. A* **103**, 921 (1999).
24. J.-J. Shiang, A. V. Kadavanich, R. K. Grubbs, A. P. Alivisatos, A. P. 1995. *J. Phys. Chem.* **99**, 17417 (1995).
25. A. L. Ankudinov, B. Ravel, J. J. Rehr, S. D. Conradson, *Phys. Rev. B* **58**, 7565 (1998).
26. A. I. Frenkel, J. J. Rehr, *Phys. Rev B* **48**, 585 (1993).
27. G. Dalba, *et al.*, *Phys. Rev. B* **58**, 4793 (1998).
28. For two atoms vibrating in their center of mass frame in an effective pair potential characterized by spring constant k, the bond frequency, $\omega = \sqrt{k/\mu}$, where μ is the reduced mass. For CdSe, $1/\mu = 1/M_{Cd} + 1/M_{Se}$ (M_{Cd} is the atomic mass of Cd). For CdSe, $\nu_{CdSe} = 4.97$ THz (*27*). For ZnS, we obtained $\nu_{ZnS} = 7.12$THz. The interatomic force constants for CdSe and ZnS are expected to be similar. If we assume that $k_{CdSe} = k_{ZnS}$, then $\left.\frac{\omega_{CdSe}}{\omega_{ZnS}}\right|_{predicted} = \sqrt{\frac{\mu_{ZnS}}{\mu_{CdSe}}} = 0.68$. In fact, $\left.\frac{\omega_{CdSe}}{\omega_{ZnS}}\right|_{observed} = \sqrt{\frac{\mu_{ZnS}}{\mu_{CdSe}}} = 0.676$. Hence, the results presented here for bulk ZnS and in (*27*) for bulk CdSe are in good agreement.

29. We thank M. Toney for discussion on PDF analysis, C. Kim for practical advice on EXAFS acquisition, and M. Zach for assistance with sample holder fabrication. SAXS data were acquired on beamline 1.4 at the Stanford Synchrotron Radiation Lab (SSRL), and we thank J. Pople. Zn K-edge EXAFS were acquired on beamline 4-3 at SSRL, and we thank M. Lattimer. WAXS data were acquired on beamline 11-ID-C at the Advanced Photon Source (APS), Argonne National Laboratory, and we thank Y. Ren and M. Beno. The U.S. Department of Energy, Office of Basic Energy Sciences, supports use of the APS (Contract No.W-31-109-Eng-38) and the SSRL (Contract No. DE-AC03-76SF00515). HRTEM was performed at the National Center for Electron Microscopy, Berkeley, CA, and we thank C. Song. Financial support for this work came from the U.S. Department of Energy, the National Science Foundation, and Lawrence Berkeley National Laboratory.